2016

Performance and modeling of paired polishing process

Tianyu Yu
Iowa State University, tianyuyu@iastate.edu

David Thomas Asplund
Iowa State University, dasplund@iastate.edu

Ashraf F. Bastawros
Iowa State University, bastaw@iastate.edu

Abhijit Chandra
Iowa State University, achandra@iastate.edu

Performance and modeling of paired polishing process

Abstract
Paired polishing process (PPP) is a variant of the chemical mechanical polishing process which facilitates defect mitigation via minimization of maximum force as well as effective planarization via profile driven determination of force gradient. The present embodiment of PPP machine employs two polishing wheels, radially spanning the wafer surface on a counter-gimbaled base. The PPP machine is deployed to experimentally investigate the role of the process parameters on the surface roughness evolution, and the effective material removal rate. Two sets of copper and aluminum blanket layers were polished under a range of applied down force, polishing wheel speed and transverse feed rate to examine the scalability of the process parameters for different material constants. The experimental measurements along with the topological details of the polishing pad have been utilized to develop a mechanistic model of the process. The model employs the soft wheel-workpiece macroscopic contact, the polishing wheel roughness and its amplification to the local contact pressure, the kinematics of abrasive grits at the local scale, and the collective contribution of these individual micro-events to induce an effective material removal rate at the macroscale. The model shows the dependence of the material removal on the ratio of wheel rotational to feed speed for the PPP process, in a form of an asymptote that is scaled by the surface hardness of each material. The PPP machine exploits this insight and utilizes an oblique grinding technique that obviates the traditional trade-off between MRR and planarization efficiency.

Keywords
Paired polishing process, Total material removal, Material removal modeling, Surface roughness, Chemical Mechanical Planarization, Precision manufacturing

Disciplines
Aerodynamics and Fluid Mechanics | Manufacturing | Other Aerospace Engineering | Other Mechanical Engineering

Comments
This is a manuscript of an article from International Journal of Machine Tools and Manufacture (2016). The final publication is available via: http://dx.doi.org/10.1016/j.ijmachtools.2016.07.003.

Performance and Modeling of Paired Polishing Process

Tianyu Yu[1], David T. Asplund[2], Ashraf F. Bastawros[1,2,*], Abhijit Chandra[2,1]

[1]Dept. of Aerospace Engineering, [2]Dept. of Mechanical Engineering,

[1]Howe Hall 1200, Iowa State University, Ames, IA 50011, USA

[2]Black Engineering 2025, Iowa State University, Ames, IA 50011, USA

**Corresponding author,*

Email: bastaw@iastate.edu; Phone: +1-515-294-3039

Co-Authors, Email tianyuyu@iastate.edu, achandra@iastate.edu

December 2015

Author's copy

For prospective publications in the IJ Machine Tools & Manufacture

This is a manuscript of an article from *The International Journal of Advanced Manufacturing Technology* (2016). The final publication is available at Springer via http://dx.doi.org/ 10.1007/s00170-016-9085-3.

Abstract

Paired polishing process (PPP) is a variant of the chemical mechanical polishing process which facilitates defect mitigation via minimization of maximum force as well as effective planarization via profile driven determination of force gradient. The present embodiment of PPP machine employs two polishing wheels, radially spanning the wafer surface on a counter-gimbaled base. The PPP machine is deployed to experimentally investigate the role of the process parameters on the surface roughness evolution, and the effective material removal rate. Two sets of copper and aluminum blanket layers were polished under a range of applied down force, polishing wheel speed and transverse feed rate to examine the scalability of the process parameters for different material constants. The experimental measurements along with the topological details of the polishing pad have been utilized to develop a mechanistic model of the process. The model employs the soft wheel-workpiece macroscopic contact, the polishing wheel roughness and its amplification to the local contact pressure, the kinematics of abrasive grits at the local scale, and the collective contribution of these individual micro-events to induce an effective material removal rate at the macroscale. The model shows the dependence of the material removal on the ratio of wheel rotational to feed speed for the PPP process, in a form of an asymptote that is scaled by the surface hardness of each material. The PPP machine exploits this insight and utilizes an oblique grinding technique that obviates the traditional trade-off between MRR and planarization efficiency.

Keywords:

Paired polishing process, Total material removal, Material removal modeling, Surface roughness, Chemical Mechanical Planarization, Precision manufacturing

Nomenclature

A_0	Wafer- wheel Apparent contact area
A	Wafer- wheel true contact area
D	Polishing wheel diameter
d_p	Abrasive grit diameter
E_w	Wafer Young's modulus
E_s	Polishing wheel Young's modulus
$\tilde{E}$	Effective contact modulus
F	Wafer- wheel total contact force
f_p	Average force per abrasive grit
H_0	Wafer material hardness
ℓ_c	Wafer- wheel contact length
P	Pad asperity contact pressure
P_o	Wafer- wheel apparent contact pressure
σ_0	Wafer material flow stress
r_c	Particle-wafer process zone contact radius
r_{asp}	Pad asperity average contact radii
t_d	Dwell time
V_f	Wheel transverse speed
V_s	Wheel speed
V_w	Wafer speed

Vol_p	Single grit volume remove rate
W	Wheel width
α_{asp}	Pad morphology dimensionless constant
β	Scaling factor
β_c	Ploughed trenches overlapping ratio
λ_p	Inter-particle spacing
ν_w	Wafer Poisson's ratio
ν_s	Wheel Poisson's ratio
ξ_{asp}	Pad asperity density per unit area
ξ_p	Active particle density per unity area
ρ_p	Abrasive volumetric particle density
δ_c	Particle-wafer penetration depth

1. Introduction

The chemical mechanical polishing (CMP) process for microelectronic processing has shown tremendous increase in volume, as well as the number of CMP steps per wafer, which has been necessitated by the global planarity requirements in semiconductor industry. Concurrently, however, process complexity in terms of the number of CMP steps and uniqueness of each step has also increased by orders of magnitude [1-4]. The CMP process has evolved through multiple generations, dated back to 1969 [5, 6], employing a large pad and a single wafer carrier that rotated about their respective axes. Over the past three decades, CMP machine design has undergone about five generations of re-design [7-11], each generation emphasizing different aspects ranging from high throughput, ease of fault diagnosis and reduction of down time. As an industrial process, CMP is expensive both in terms of capital cost, and cost of operation. Recently, with shrinking feature size (currently <15 nm), CMP has also been mired by defectivity (e.g., scratch and film delamination) [2-4] at a multiplicity of length-scales ranging from within wafer nonuniformity at wafer scale, within die nonuniformity at die scale to defectivity concerns at feature or nano-scale. Waviness reduction over a wide range of wavelengths still remain an expensive proposition. Reliability of the CMP process remains a primary goal, and currently the CMP industry is attempting to reduce defectivity and enhance reliability from all possible angles. Major development effort remains focused on consumable, (e.g. pads, slurries, wafer carrier, etc.), as well as CMP platform modification to overcome defectivity [12].

A review of the CMP process attributes show two major process needs. These are (i) the removal of long wavelength waviness, arising from wafer cutting process, and (ii) the retention of lower defectivity and scratches. The proposed PPP is an attempt to provide an economic, yet defect retardant process. The process utilizes pairs of fast rotational wheels with a shallow contact with the machined surface to reduce scratches and improve planarization. The orthogonality of the wheel rotational motion and the transverse velocity motion (or motion of the wheel center) introduces obliqueness that facilitate long wavelength waviness reduction. This paper focuses on the role of the process parameters on controlling the material removal rate (MRR) and its effectiveness in removal of surface waviness. The details of the process are summarized in Section 2. The developed experimental protocol and consumables are discussed in Section 3. A detailed mechanistic model is developed in Section 4, based on the experimental results of two different materials (i.e. Cu and Al blanket films) to elaborate the role of the process parameter and

consumables on the process performance. Section 5 summarizes the experimental measurements and provide comparison with the developed mechanistic model.

2. Paired Polishing Platform

The employed PPP platform is illustrated in Fig. 1(a), showing the main control elements and the process kinematics. Details of platform can be found in [13, 29]. Each polishing wheel is independently controlled to span the wafer surface, either in tandem or concentric. However, concentric motion is preferred to maintain system stability. Each wheel's motor is supported on a load cell, fixed to the transverse mechanism to independently measure the normal contact force at the polishing wheel/wafer interface. The two wheel assemblies are supported on a vertical crosshead with possible displacement or contact load control. The wafer holder assembly is supported by a gimbal mechanism to rebalance the forces between the polishing wheels and avoid scratches. The lower platen, supporting the wafer holder and the gimbal mechanism, is supported by a thrust bearing to the frame. The slurry dispensing assembly is mounted to the frame and directed at the wheel/wafer interface. The dispensing nozzle is mounted to the bracket of the polishing wheel motor.

The main process parameters, elaborated on Fig. 1(b), are the contact force F between the wafer and the polishing wheels, the wheel speed V_s, the wafer speed V_w, and the wheel transverse feed rate V_f. All polishing tests are conducted with open loop control on F and V_f.

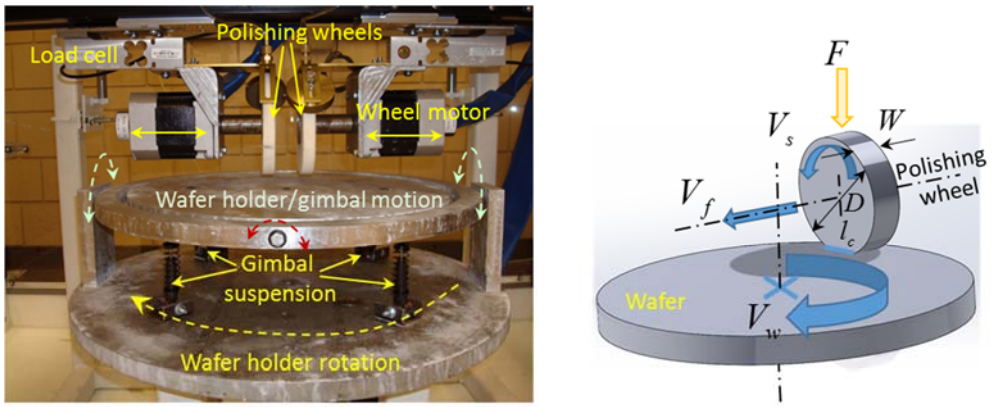

(a) (b)

Figure 1: (a) Optical view of the PPP system showing the relative motion of the main components (dashed arrows). Vertical crosshead provides down feed. Polishing wheels translational stages provides transverse feed and table rotation provides progressive whole surface polishing. (b) Illustration of the obliqueness in process kinematics

3. Experimental Protocol

3.1 Materials and Consumables

An experimental parametric study is performed to determine the performance of the PPP. Two sets of blanket copper and aluminum surfaces are examined to show the universal applicability of the process and the modeling framework. The surfaces are generated from sheet stock of 3.2 mm, 6061-T4 aluminum alloy and 99.99% oxygen free copper. The initial surface roughness (RMS: measured by the root mean square deviation of surface profile; ISO 4287-1998) is about RMS=300 nm for copper and RMS=460 nm for aluminum, within a 1.4 x 1.4 mm^2 window. Though, the global planarity of the as-received surfaces was poor, showing significantly high level of waviness at longer wavelengths (8-20 mm). Two sets of wafer diameters of 40 and 150 mm are machined to examine the process parameter space with the least amount of materials and polishing time. The large 150 mm wafers are used to assess the overall planarization capabilities of the process, while the small 40 mm wafers are used to study the role of the process parameters on MRR, and the local roughness evolution. The entire data set for the aluminum wafers are presented. The copper data are presented to show the universality of the developed model and its scaling with the polished surface hardness.

A suspended 1 μm agglomerate alumina particle slurry with pH 8.5 and solids content by weight of 15% (Ultra-Sol M5PS, Eminess Technologies Inc.) is utilized, after being diluted with deionized water at 1:8 ratio. This provide particle volume ratio of 0.5% approximately. Most of the testing were conducted with such large particle slurry to arrive at a measurable material removal rate for comparison with the model. For near CMP surface finish quality, a subset of experiments were conducted with 0.05 μm colloidal silica slurry (Dow Klebosol 1508-50) with pH 10.9 and 30% solid concentration. After dilution, the particle volume ratio is about 2%. The polishing wheels are impregnated felt (Spartan Felts) of diameter D = 127 mm, width W= 12.7 mm thick and 12.7 mm arbor hole. Micro-indentation testing of the pad exhibited an effective elastic modulus of $E_s = 10$ MPa and Poisson's ratio $\nu_s = 0.5$. Details of the pad surface asperities are shown in Fig. 2. The analysis of the wheel surface roughness from the SEM images and 3D surface topology image [24, 25], provided measures of the average asperity density per unit area, $\xi_{asp} = 17$ mm^{-2}, and the average asperity radii, $r_{asp} \approx 15$ μm. The asperity density is estimated from the number of summits intersection with a cut plane, at a distance of $3\,r_{asp}$ from the highest peak

in the image, indicated by the shaded plane on Fig. 2(b). The selected cut plane height is approximate and is substantiated form the full statistical analysis of the pad surface roughness [16, 26]. The mean curvature (average of the two principal curvatures) for each asperity is evaluated within the image. The representative r_{asp} of the pad is the average of all asperity radii within the image.

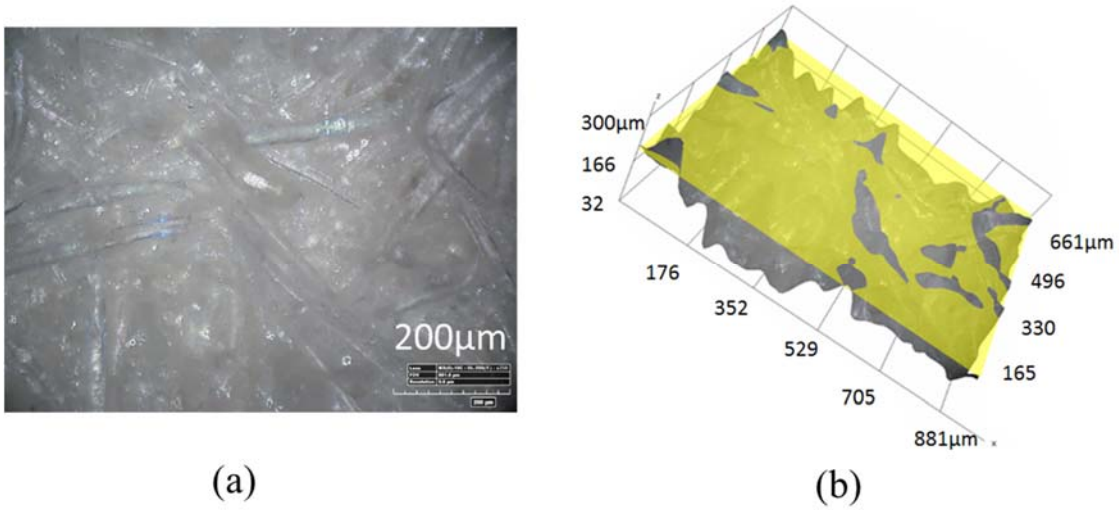

Figure 2: Topology of the utilized polishing wheel. (a) Optical micrograph of the surface topology. (b) Three dimensional optical micrograph of pad asperity, showing the pad density, ξ_{asp} at a critical height of three times the asperity radius (shaded plane).

3.2 Experimental Procedure

The process control parameters are V_s, V_s and F. The 150 mm wafers are utilized to evaluate the overall process planarization performance. All testing on the 40 mm wafers are conducted at a fixed wafer support position, and holding the wafer rotation, to reduce the initial number of the process parameters. In each experiment, either a large 150 mm wafer or a pair of blank wafers of 40 mm is mounted on the wafer platen. The large wafer is scanned outward by the pair of wheels in a single path. For the 40 mm wafers, a polished trench is generated in each wafer, spanning the entire wafer and having a width equal to the wheel- wafer contact length, as depicted in Fig. 5. All tests were conducted with the 1 µm slurry to get a measurable total material removal (TMR). A limited set of experiments on the Al-wafer were carried out with the 0.05 µm to show

the near CMP performance. All reported experimental conditions are summarized in Table 1.

The polishing wheels are soaked in DI water for 24 h before testing. After mounting to the arbor, the wheels are then spun for 5 minutes to expel the excess water. Then, the wheels start to receive the slurry for few minutes before the start of the test. For the large wafer, the wheels are moved in tandem first to cover the center of the wafer, then switched to move in concentric opposed motion. However, via optimization, the initial central area of question can be limited to a single die and both wheels can move in opposite direction. Such set-up is typically preferable compared to typical edge exclusion (involving many more dies) used in conventional CMP. For the small wafers, each wheel comes in contact with one edge of the pair of small wafers to establish contact and set the initial contact force, while being spun. The cross-head translational stages apply the transverse feed until the wheels pass beyond the small wafer surface, on to the mounting wafer holder.

All polished surfaces are analyzed by noncontact surface profilomter based on white light interference (Zygo NewView 6300). Three dimensional surface topological maps were acquired at different magnifications to analyze the resulting surface roughness. A Gauss spline based high pass filter is utilized with the cut-off wavelength of 80 μm to assess the roughness a 1.4 x 1.4 mm^2 area (ISO 4287:1998, and ISO 11562:1998). For the large wafer profile analysis, a stitched window of 140 x 1.4 mm^2 is utilized. Three sets of measurements are carried out on each surface. The presented data in Figs. 6-10 represents the average of these measurements with the range of data within +/- one standard deviation indicated.

4. Mechanistic Process Modeling for Material Removal Rate

The PPP exhibit unique process kinematics, wherein the polishing wheel traverses the wafer surface in a spiral feed with an effective radial and angular motion. The polishing pad is highly deformable porous solid with complex topology [24, 25]. A modeling framework should embrace these unique geometric and kinematics features, even with an effective mean representation. The model attempts to establish the load transfer from the global applied load on the polishing wheel spindle, F to the local force per abrasive particle, f_p. To accomplish such objective, the model embraces (i) the soft wheel-workpiece macroscopic contact, (ii) the polishing wheel roughness and its amplification to the local contact pressure, (iii) the kinematics of abrasive grits at the local scale, and (iv) the collective contribution of these individual micro-events to

induce an effective material removal rate at the macroscale. The model is simplified for the special case of stationary wafer, wherein $V_w = 0$, so as to develop an expression for the total material removal within the formed macroscopic trench on the 40 mm small wafers (cf. Fig. 5). The modeling results are compared to the experimental measurements in Section 5.

4.1 Pad-workpiece macroscopic contact

The polishing wheel interaction with the wafer can be modeled as a cylindrical contact with a flat plate. The apparent contact area, A_0 is $A_0 = \ell_c W$, wherein ℓ_c is the contact length between the wafer and the wheel, marked on Fig. 5. The average contact pressure within the contact area, for an applied force, F, is $P_0 = F/A_0$. From contact mechanics [14], ℓ_c is determined by F, the wheel diameter, D and the elastic properties of the two mating surfaces such that;

$$\ell_c = \sqrt{\frac{8DF}{\pi W \tilde{E}}} \tag{1}$$

Here, $\tilde{E}$ represents the elastic properties of the mating surfaces as an effective contact modulus;

$$\frac{1}{\tilde{E}} = \frac{1-\nu_s^2}{E_s} + \frac{1-\nu_w^2}{E_w} \approx \frac{3}{4E_s} \tag{2}$$

Wherein the polishing wheel modulus, E_s is much smaller than the workpiece modulus, E_w. ν_s and ν_w are the Poisson's ratios for the polishing wheel and workpiece respectively.

4.2 Role of polishing wheel roughness

The true forces on asperity summits are controlled by the polishing wheel roughness. An analytically attractive approach proposed by Greenwood and Williamson [14, 15] is to address the roughness through an asperity density per unit area, ξ_{asp} with an average asperity radii, r_{asp}. These quantities can be estimated from the polishing wheel morphology, as discussed in Section 3.1 and

shown in Fig. 2. The true contact area, A will arise from the evolution of the summit deformation under the applied load, such that;

$$A = \alpha_{asp} \left(\frac{P_0}{\tilde{E}} \right)^{\frac{2}{3}} A_0 \,, \qquad \alpha_{asp} = \pi \left(\frac{9\, r_{asp}^2\, \xi_{asp}}{16} \right)^{\frac{1}{3}} . \tag{3}$$

α_{asp} is a dimensionless constant, which depends on the polishing wheel morphology. As a first approximation, it could be treated as a constant for a given pad morphology. Though, an evolution equation could be invoked [16] to account for the pad wear and the associated surface morphology evolution. While important, the polishing wheel wear is beyond the scope of this work.

The average contact pressure, P within the pad asperities will be amplified through the reduction of the true contact area, such that;

$$P = \frac{P_0 A_0}{A} = \frac{1}{\alpha_{asp}} \left(\tilde{E}^2\, P_0 \right)^{\frac{1}{3}} \tag{4}$$

4.3 Abrasive distribution under the wheel

The abrasive volumetric particle density, ρ_p would provide an approximate estimate of the inter particle spacing. Assuming, closed packed simple cubic arrangement and spherical abrasive particles with diameter, d_p, the inter-particle spacing, λ_p could be estimated as:

$$\lambda_p \approx \left(\frac{\pi d_p^3}{6\rho_p} \right)^{\frac{1}{3}} \tag{5}$$

λ_p represents a uniform distribution of the abrasive grit in both the feed and transvers direction of the polishing process. For the utilized 1 μm slurry ($d_p = 1\,\mu\text{m}$ and $\rho_p \approx 0.5\%$), the inter-particle spacing is about $\lambda_p \approx 5$ μm. While this is a reasonable approximation for face-down polishing to estimate the active abrasive particle per unit area [17, 27], tangential polishing wheel seems to exhibit different behavior. Fig. 3(a) is an optical micro-graph of the polishing trace marks. Careful examination of these trace marks reveals pattern of imbedded particles within the surface.

The inter-particle spacing along the tangential path is about $50\lambda_p$. Such long range correlation might imply that every fiftieth particle in the tangential direction is participating in the cutting process. It could be argued that every active cutting particle, shield the trail of particles in its shadow until a tangential arc-length on the tangential cutting trajectory is attained. This shielded tangential arc-length is geometrically equivalent to a full indentation depth of the abrasive particle into the wafer, δ_c. Fig. 3(b) illustrates the proposed process kinematics.

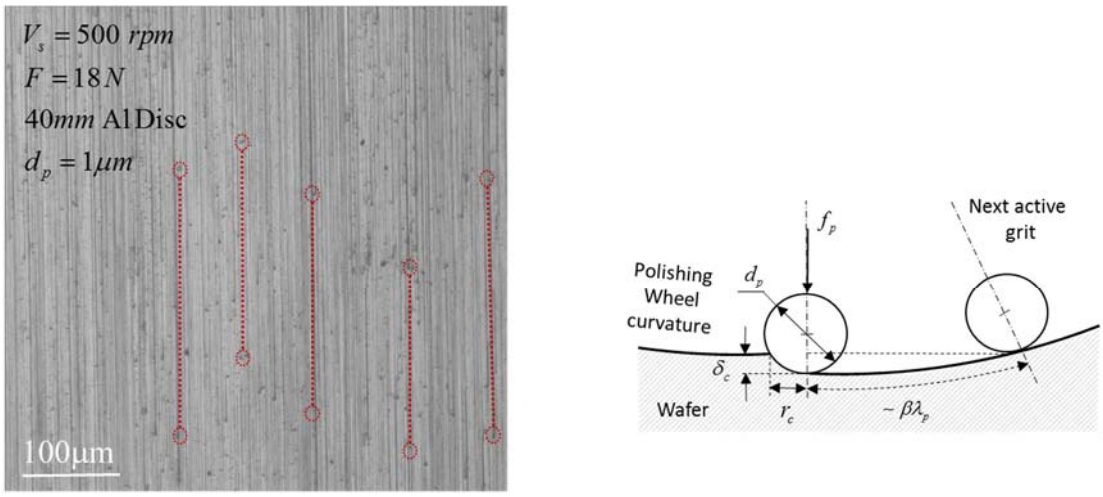

(a) (b)

Figure 3: (a) Polished Al surface with 1 μm slurry showing effective cutting length along V_s direction is about 250 μm. (b) Sketch of the proposed active cutting grit, and the shadow trail of length $\beta\lambda_p$ in its wake, until a new grit penetrate the surface, $\left(\beta \sim 50 \text{ for } d_p = 1\,\mu m\right)$.

Additional examination of polished surfaces under different loading levels and wheel RPM revealed weak variation of this long-range correlation of the active polishing particles. Accordingly, the active particle density per unity area, participating in the polished process can be estimated as,

$$\xi_p \approx \frac{1}{\beta\lambda_p^2} = \frac{1}{\beta}\left(\frac{6\rho_p}{\pi d_p^3}\right)^{\frac{2}{3}} \qquad \textbf{(6)}$$

Eq. (6) shows the scaling of the active abrasive grit with the slurry volumetric density and the abrasive particle size, through the scaling factor $\beta(\sim 50)$, that represents the active cutting grits along the ploughing direction. For the 0.05 slurry ($d_p = 0.05\,\mu m$ and $\rho_p \approx 2.0\%$), the inter-particle spacing is about $\lambda_p \approx 0.15\,\mu m$. The image analysis of the polished surface showed the 0.05 μm particles as clusters (agglomerated) and the inter-particle spacing along the tangential path is about $650\lambda_p$. The particle agglomeration process would change the scaling factor by an order of magnitude for this case $(\beta \sim 650)$. The scaling factor β is a mere reflection of the process kinematics and slurry electrochemical stability and should be examined further experimentally. However, as it will be discussed in Section 5, no other fitting parameters would be required.

4.4 Material removal per grit

For each active cutting particle, the associated material removal is controlled by the applied local pressure, P, the wafer material intrinsic resistance to mechanical flow as measured by the material flow stress, σ_0 or alternatively by hardness, H_0 (note that $H_0 \approx 3\,\sigma_0$, for metals [18]), and the particle geometry, d_p. Assuming three body contact to support the local pressure through the polishing wheel-particle-wafer contact, and through the polishing wheel-fluid-wafer contact, the force per particle, f_p can be assessed by,

$$f_p = \frac{\pi}{4} P d_p^2 \tag{7}$$

Assuming statically admissible state of stress under the abrasive grit, f_p is balanced by the radial stresses on the indentation surface area [17, 19, 27]. This can be approximated by the projected particle-wafer contact area, multiplied by the wafer hardness H_0 [20]. Accordingly, the particle-wafer process zone contact radius, r_c can be estimated as,

$$r_c = \left(\frac{2 f_p}{\pi H_0} \right)^{\frac{1}{2}} \tag{8}$$

And the associated particle-wafer penetration depth can be also estimated as

$$\delta_c = \frac{2 f_p}{\pi d_p H_0} \tag{9}$$

These geometric parameters are depicted on Fig. 3(b). In modeling the MRR, the chemical effect akin to the slurry surface interaction. It is generally accepted that the chemical reaction during the CMP process might either soften the top surface layer, and/or dissolve the formed debris from the ploughing and removal process [28]. If the chemical effect is softening the surface layer, then H_0 in Eqs. (8) and (9) should be the hardness of such softened (chemically reacted) film. However, if the chemical effect is to dissolve the removed derbies, then Eq. (9) still holds as representation of the extent of indentation depth into the polished surface. Thus a quasi-coupled chemical-mechanical modeling approach is pursued here, where the chemical effects influence the mechanical action, but not vice versa.

To arrive at a general expression for the MRR, each active abrasive grit is consider to generate a trench having $2 r_c$ width and δ_c depth. Accordingly, the rate of volumetric removal per particle, Vol_p can be estimated as,

$$Vol_p = r_c \, \delta_c \left(V_s \pm V_w \right) \tag{10}$$

The sign is determined from the relative direction of the two tangential speeds. The "+" sign is reserved for an opposing tangential speeds. The "–" sign when they are in the same direction. For the examined stationary wafer, $V_w = 0$.

4.5 Process material removal rate

The effective process MRR is the summation of the rate of volumetric removal per particle Vol_p for all the participating particles in the cutting process (measured by the density of the active abrasive particles ξ_p) within the true pad-wafer contact area A. Thus, the MRR can be expressed in terms,

$$MRR = A.\xi_p.Vol_p \tag{11}$$

The dwell time t_d defines the exposure time of every spatial location within the wafer surface to the polishing wheel. For the special examined case of stationary wafer ($V_w = 0$), wherein a macroscopic trench is formed (cf. Fig. 5), t_d is given by:

$$t_d = \frac{W}{V_f} \tag{12}$$

For the formed trenches, TMR for points within the centerline of the trench will be the time-integral of the MRR at such location, averaged over the wheel-wafer contact area, A_0. Employing, Eqs. (1)-(10) into Eqs. (11) and (12), the TMR as a function of the process parameters is given by:

$$TMR = \frac{MRR.\, t_d}{A_0} = \frac{5\xi_p d_p^2}{\sqrt{\alpha_{asp}}}\left(\frac{E_s^{11}}{H_0^{18}}\right)^{\frac{1}{12}}\left(\frac{W^5 F^7}{D^7}\right)^{\frac{1}{12}}\left(\frac{V_s}{V_f}\right) \tag{13}$$

The expression for TMR captures the confluence of the microscopic pad topology and slurry, the polished wafer properties, the macroscopic pad geometry and the applied force, as well as the relative velocity ratio. The model perdition is compared with the experimental results on Fig. 6 for the applied force, and on Fig. 8 for the transverse feed rate. Though, the dependence of TMR on the ratio of V_s/V_f provides broad range of process parameters, wherein as shown in Fig. 10, the TMR can be achieved with different system dynamics and prospective surface roughness enhancement. Additionally, if the dependence on the applied force applied force, F is replaced with the mean contact pressure, P_0 employing Eq. (1), a near linear dependence on the applied pressure is attained. This will render Eq. (13) to have a similar form to the classical Preston equation for polishing materials [21] with linear dependence of MRR on the applied pressure and the relative polishing speed.

5. Results and Discussion

The modeling framework suggest that the leading process parameters that control the TMR are the applied down force F and the velocity ratio V_s/V_f. The experimental plan was devised to examine the role of each of these parameters on the TMR as well as the resulting surface roughness.

5.1 PPP process planarity:

Preliminary experimental polishing results of the large 150 mm Al-wafer is shown in Fig. 4, after passing through the wafer center with the wheels in tandem and then a single polishing sweep of the whole surface, with the wheels in opposite direction. Interestingly, the as received

surface has an initial waviness or a total thickness variation (TTV) of approximately 80 μm; normal to the rolling direction. While a single sweep of surface polishing is carried out with a table rotation of 50 rpm, and a transverse feed rate of $V_f = 0.21$ mm/s, the surface TTV is reduced to less than 12 μm. Edge singularities are omitted from this graph. This promising result shows the global planarity potential of the PPP platform to attain tight TTV over a 150 mm wafer span or longer. It could be further improved by having a variable transverse feed speed V_f to yield a constant dwell time on each point of the wafer. Prospectively, the transverse feed could be preprogramed to overcome an initial surface waviness with variable MRR over each zone.

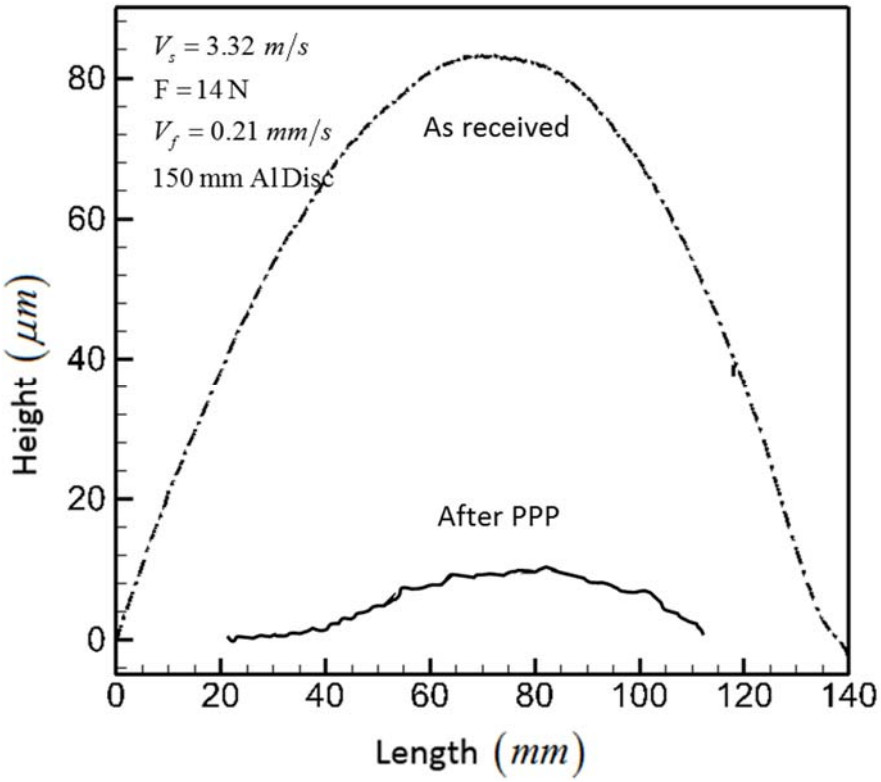

Figure 4: Evolution of total thickness variation (TTV) over 150 mm Al-disc after a single sweep of the surface on the PPP platform showing reduction of TTV from more than 80 μm to less than 12 μm. Table rotated at 50 rpm.

The local surface roughness is shown in Fig. 5 after polishing pairs of 40 mm stationary wafers with 1 μm slurry, forming a polished trench across. The machined trench has a height, representing the TMR, which will be compared with the model prediction of Eq. (13). The trench

width is equivalent to the contact length, ℓ_c, given by Eq. (1). The as received surface (zone I on Fig. 5) has initial RMS=327 nm. The surface roughness after the PPP, evolved to RMS=5 nm after a single sweep with the polishing wheel. A middle-line profile is shown in both cases.

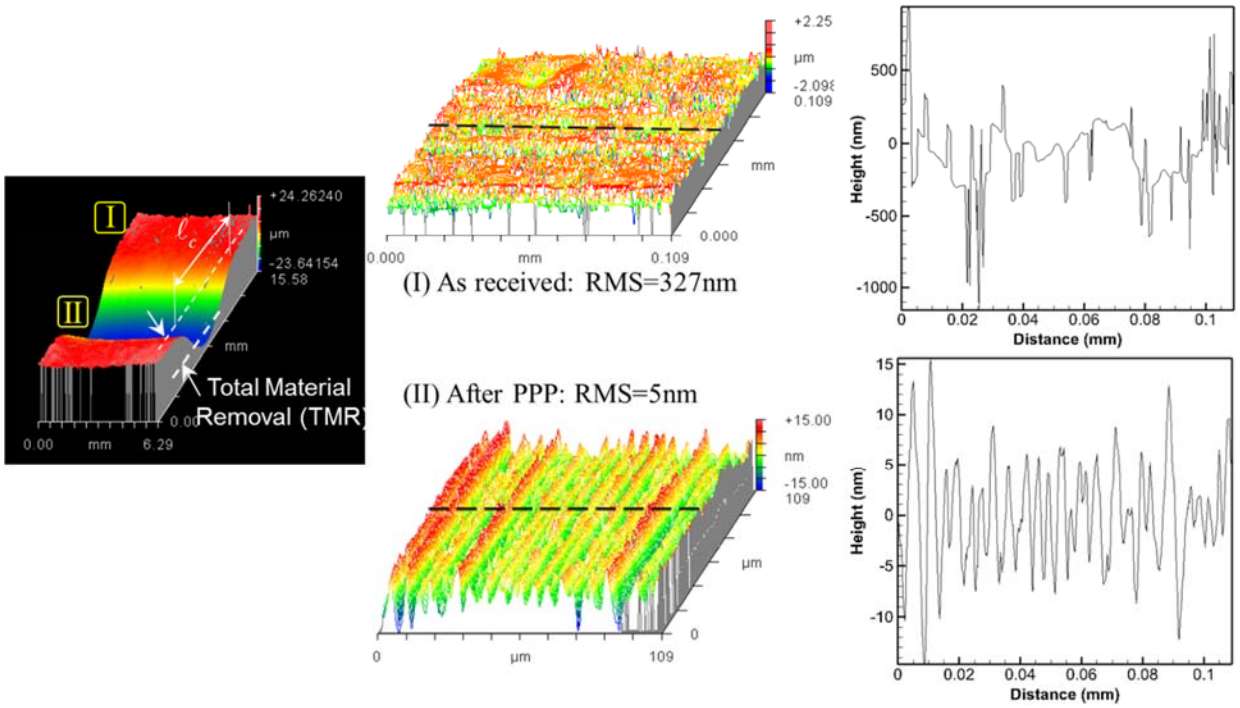

Figure 5: Polishing results of 40 mm Cu-disc using 1μm slurry, showing local from RMS= 327 nm to less than RMS=5 nm after a single PPP sweep.

5.2 Role of contact load, F on polishing behavior

A set of 40 mm Al wafers were polished under a range of applied contact load of 4-18 N per wheel. A polishing wheel speed of $V_s = 3.32$ mm/s (500 rpm) and a transverse feed of $V_f = 0.21$ mm/s were maintained during all tests. Since each experiment would yield two wafers (one per wheel), each testing condition was repeated twice, yielding four sets of polished surfaces. A set of three samples where polished at each load. Figure 6 summarizes the experimental measurements of the TMR with the applied contact load for two sets of slurries. The TMR variation is measured from three points along the machined trench profile, marked on Fig. 5 as the depth of the polished trench. The error bar represents one standard deviation from the mean value. The error bar on the applied force derived from the bounds of the oscillatory contact force, arising from the polishing wheel/wafer contact dynamics. The prediction of Eq. (13) for TMR is also shown on

Fig. 6, employing the substrate properties ($H_0 \approx 270$ MPa for 6061-T4 aluminum alloy and 340 MPa for high purity copper). Utilizing a scaling parameter for the model results of order unity (0.92), the model prediction remarkably fits both the trend and the amplitude of the experimental data for both slurries without any additional corrections. Accordingly, utilizing the average distribution of pad asperities and the average distribution of the slurry particles, scaled by the parameter; β provides a simplified approach to accurately predict the MRR, without the need to account for the full statistical distribution of the abrasive particles and the pad asperities, and then numerically solve the wheel/wafer contact evolution [16].

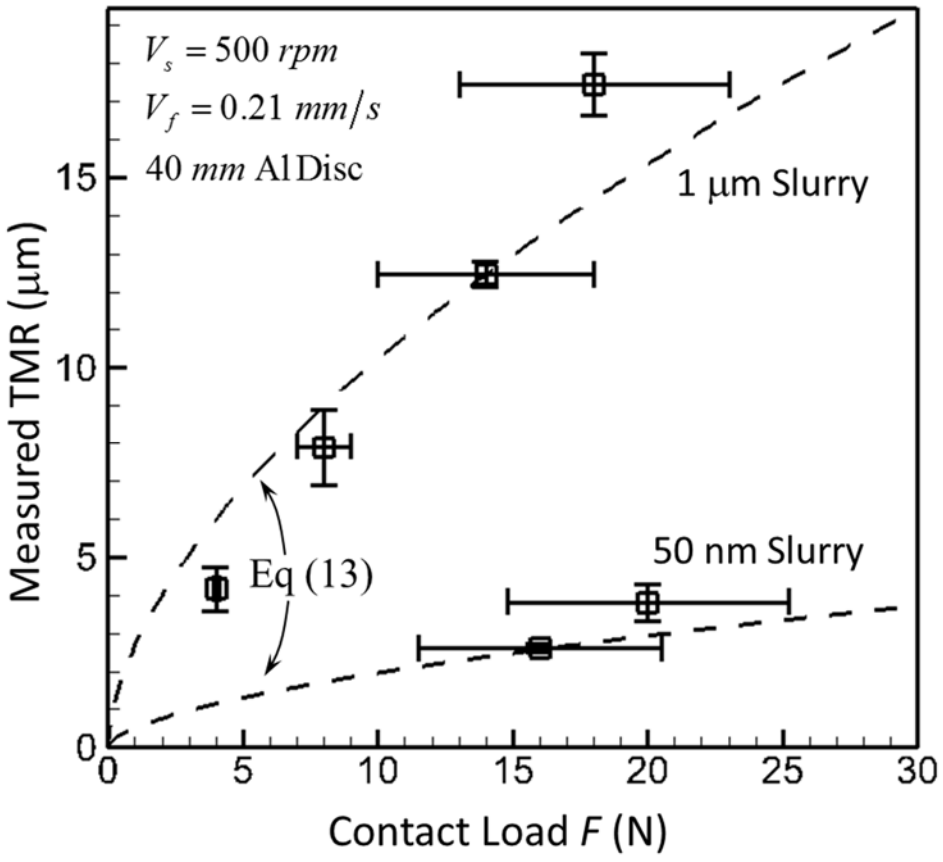

Figure 6: Role of applied contact load on the variation of TMR. The model prediction of Eq. (13) remarkably fit the experimental data with scaler of order unity for slurries with two different abrasive sizes.

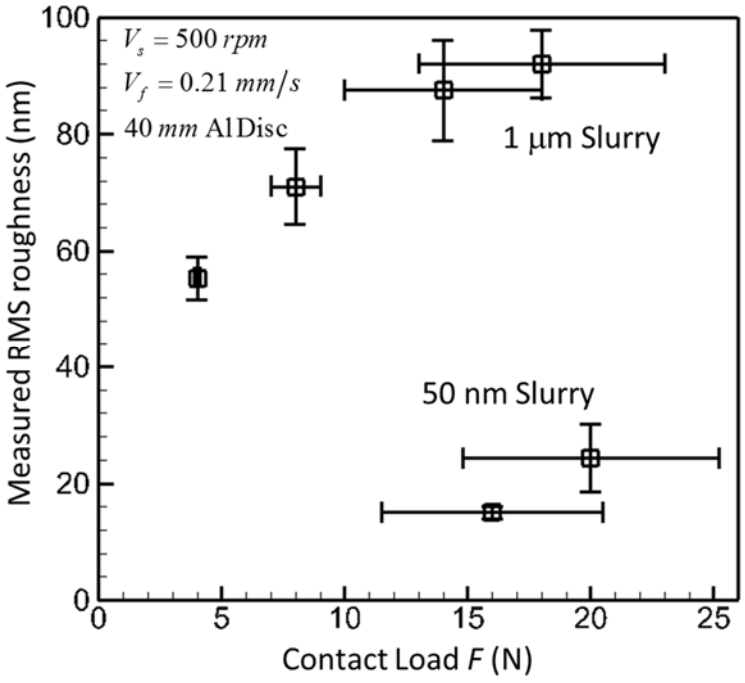

Figure 7: Role of applied contact load on the variation of RMS roughness, showing persistent increase with the load. RMS roughness is measured over an area of 1.4×1.4 mm^2

Figure 7 summarizes the evolution of RMS roughness with the applied contact load on the Al wafer. For the 1 μm slurry, the roughness shows persistent increase with the load, ranging from RMS= 55 nm to 92 nm, measured over 1.4×1.4 mm^2 window. Such trend could be rationalized as a result form the dynamics of the polishing wheel/wafer surface. As the applied force is increased, the tangential forces is also increased, leading to an increase of the effective length scale for micro-adhesion and micro-slip [14, 22]. Such local disturbances lead to increase of the surface roughness. For the 0.05 μm slurry representing near CMP quality, close to six times reduction of roughness could be observed. Though, at lower loads, the roughness was within the instrumentation measurement noise. This range of roughness performance shows the potential for the PPP to reach the critical CMP process performance.

5.3 Role of transverse feed rate, V_f on polishing behavior

A set of 40 mm Al wafers were polished under a range of the transverse feed rate V_f . The transverse feed rate controls the dwell time of the polishing wheel at any spatial location of the

polished surface and thereby would reduce the TMR. All tests were carried out at $V_s = 3.32$ mm/s and $F = 18$ N. Four different transverse feed speed; $V_f = 0.1 - 0.9$ mm/s were utilized. Fig. 8 shows the measured variation of TMR with the transverse feed rate. The model prediction of Eq. (13) is also plotted on Fig 8. The model predicts well the inverse dependence of TMR on V_f.

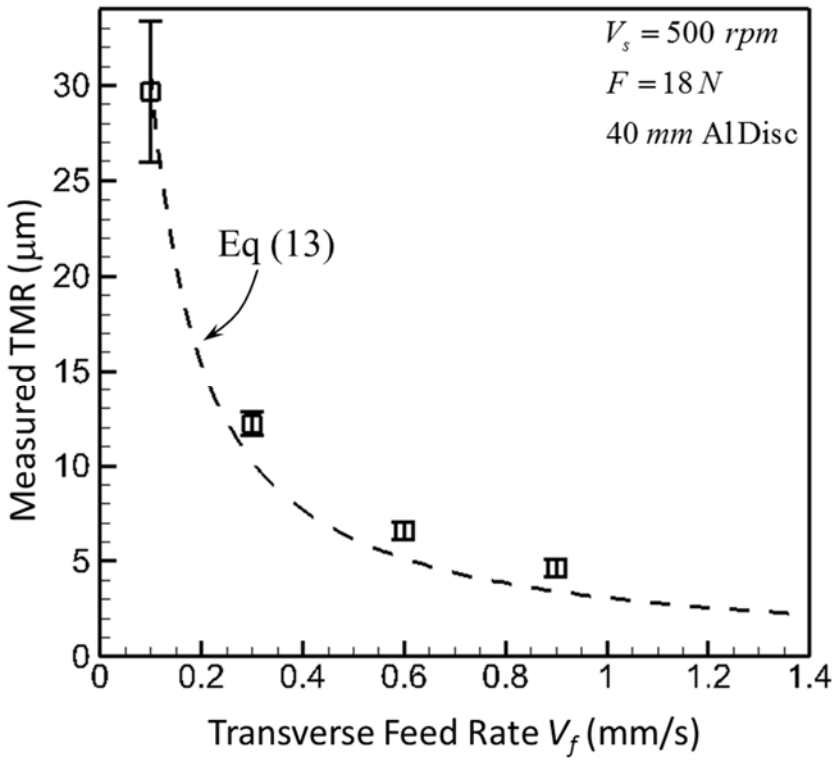

Figure 8: Role of transverse feed rate on the variation of TMR, showing a marked reduction due to the dwell time reduction. The model prediction of Eq. (13) remarkably show the inverse proportionality with V_f .

Fig. 8 shows unique feature of the variability in the measured TMR as it is reduced with V_f and exhibited a narrower range. Though the measured roughness at such applied contact load was almost independent of V_f . For the 1μm slurry, RMS was about 100 nm with 10 nm standard deviation, which is the same level for a similar contact load on Fig. 7. Such effect of V_f might be similar to the effect of lateral vibration of the workpiece, normal to the grinding direction, wherein an improvement in planarity and MRR has been reported [23].

5.4 Role of polishing wheel RPM, V_s on polishing behavior

This section summaries the results of Cu and Al 40 mm wafers as the characteristics of the trend were surprising but quite repeatable for the two materials with different hardness. All polishing experiments were carried out with the 1 μm polishing slurry and under a range of the transverse feed rate V_s. A range of rotational speed of 500-2000 rpm ($V_s = 3.3 - 13.3$ m/s) were employed, while maintaining the transverse feed rate at V_f =0.21 mm/s and contact load at F = 20 N. The Cu wafers were primary polished at the higher range V_s to repeat the same TMR saturation trend observed for Al. Fig. 9 summarizes the measured variation of TMR with V_s. An initial increase of TMR can be identified for each case. Then a plateau level for TMR is attained thereafter. The model prediction of Eq. (13), is represented by a solid line, and shows the expected linear dependence on V_s for both cases, but with different slopes that scale with H_o. Though, the devitaion from such linear trend suggests the changes of the process kinematics and the existance of a limit on the domain of validity of Eq. (13). In particular, Eq. (13) suggest the dependence of TMR on the ratio of V_s/V_f . Holding V_f for the experimental set of Fig. 9 would yield different ratio of V_s/V_f for each of the examined cases. Considering the particle kinematics, the whole wheel has to move a lateral distance greater than individual particle process zone, or distance of order $2-4\ r_c$, while individual grit clears the tangential travel span within the contact area ($\sim \ell_c$). This kinematical statement can be expressed in terms of a particle dwell time under the pad, such that,

$$\frac{\ell_c}{V_s} \geq \frac{\beta_c\, r_c}{V_f}, \quad \text{or} \quad \frac{V_s}{V_f} \leq \frac{\ell_c}{\beta_c\, r_c} \tag{14}$$

$\beta_c \approx 2-4$ is a scaling factor that defines the distance between two overlapping ploughed trenches. From the intercepts of prediction of Eq. (13) for TMR and the observed saturation level, β_c was estimated to approximately be 3 for Cu and 4 for Al. Accordingly, Eq. (14) sets the domain of validity of the model prediction of Eq. (13) for TMR dependence on V_s. Beyond this range, TMR becomes independent of V_s. The limit predicted by Eq. (14) is marked by a vertical line on Fig. 9.

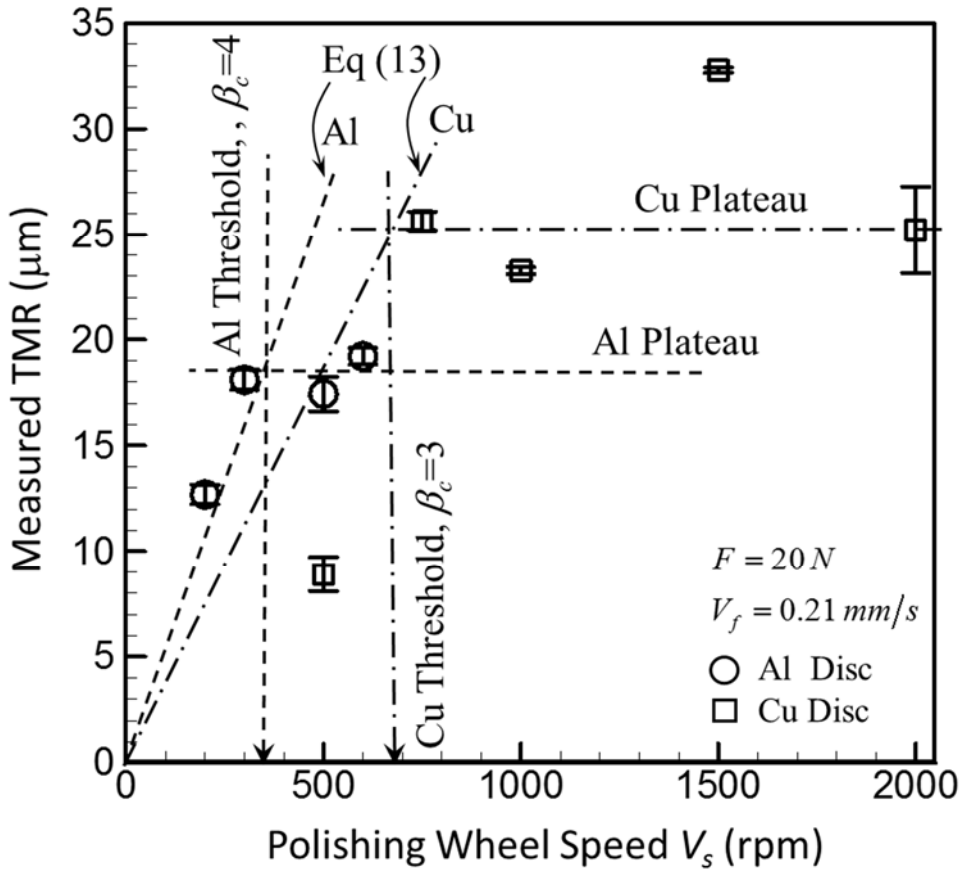

Figure 9: Role of polishing wheel speed on the variation of TMR, showing an initial increase in TMR up to 1000 rpm, TMR independent trend. The hypothesized domain of validity of the model Eq. (13) is also shown. $\beta_c \approx 2-4$ is a scaling factor that defines the distance between two overlapping ploughed trenches.

5.5 General PPP Performance

Equation (13) provides the interplay between the applied contact load, the polished material properties and the velocity ratio V_s/V_f . It should be noted that the set level of the down force F or the average contact pressure P_0 is to control the force per particle f_p . For a targeted penetration depth into the polished surface, f_p has to overcome the material resistance to flow and plough, defined by H_0 . Actually, Eq. (13) can be written in terms of P_0 such that,

$$TMR \propto \left(\frac{E_s}{H_0}\right)^{\frac{1}{3}} \left(\frac{P_0}{H_0}\right)^{\frac{7}{6}} \left(\frac{V_s}{V_f}\right) \tag{15}$$

Thus the material removal is the confluence of the V_s/V_f and P_0/H_0 ratios, for the same set of consumables including pad topology and slurry concentration. To explore such dependence, Fig.10 summarizes all the experimental data for different ranges of V_s and V_f at a given applied F for two different sets of polished material types; Cu and Al wafers with 1 μm slurry. Interestingly, for each material (e.g. Cu vs. Al), the entire experimental data set falls on the asymptote with constant P_0/H_0 ratio for materials specific properties $\left(Cu: H_0 = 340\ \text{MPa}, Al: H_0 = 270\ \text{MPa}\right)$. Accordingly, Fig. 10 provides the process domain performance for any material system by scaling the presented asymptotic correlation by the surface hardness of the new surface to be polished. For a preset applied pressure or down force, Fig. 10 provides the required velocity ratio to attain a targeted TMR. Moreover, correlation (15) is a restatement of the phenomenological Preston equation [21, 24], wherein the material removal depends linearly on the applied average contact pressure and the relative slip velocity, while the magnitude of the material removal is scaled by a material constant, typically termed as Preston constant. Correlation (15) exhibit the same trend embraced in Preston equation, but with near linear scaling with the applied pressure (exponent ≈ 1.17).

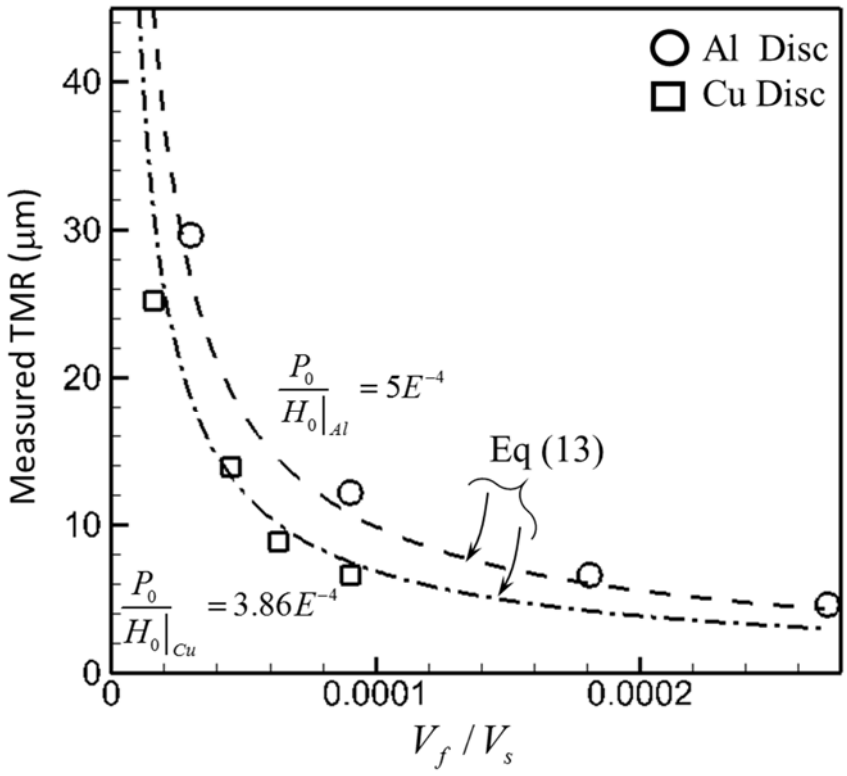

Figure 10: Process domain summarizing the entire data set for different process and material parameters. A parametric correlation can be identified for each material system, similar to the phenomenological Preston-type polishing relationship.

Fig. 10 shows another unique attribute of the PPP that is the prospect of increasing TMR at the same applied pressure by changing the V_s/V_f ratio. Thus, the corresponding MRR could be doubled by doubling velocity ratio. Such an increase in the MRR would have required an increase in F instead, but with the associated increase (almost doubling) in the surface roughness as being illustrated in Fig. 7. Accordingly, the PPP provides the pathway to trade the applied force with the velocity ratio to attain the same targeted MRR with the reduced surface roughness [29].

6 Conclusion and future work

The attributes of PPP have been investigated experimentally on two different sets of materials. An analytical model is developed, employing the details of the contact mechanics at the grit scale, the abrasive grit kinematics and the macroscopic contact of the polishing wheel/wafer.

The model shows the role of the process parameters on the evolution of MRR as well as surface roughness. The model shows a Preston-type dependence on the applied pressure and relative slip velocity, with the Preston proportionality constant being defined by the material and process parameters. Moreover, the model shows the dependence of the material removal on the ratio of wheel rotational to feed speed for the PPP process, in an asymptotic form, which scales with the surface hardness. In particular, the combined experimental and modeling results show the unique features of the PPP to trade the applied force with the velocity ratio to attain the same targeted MRR with the reduced surface roughness. Additionally, they show the proper velocity ratio V_s/V_f domain of operation for continued enhancement of the MRR, with the promise of utilizing the transverse feed speed over wheel spinning speed ratio to enhance MRR and planarization efficiency simultaneously.

ACKNOWLEDGEMENTS

This work is supported by the U.S. National Science Foundation under Grant No. CMMI-1100066. Any opinions, conclusions or recommendations expressed are those of the authors and do not necessarily reflect views of the sponsoring agencies. Few of the CMPG experiments are conducted by Hao Bai and Christopher Coppess under NSF-REU supplemental program, the authors are thankful for their work.

References

[1] R.L. Rhoades, J. Murphy, Adopting CMP processes to achieve new materials integration, Micro. 24(6) (2006) 51-54. 11444 W OLYMPIC BLVD, SUITE 900, LOS ANGELES, CA 90064 USA: CANON COMMUNICATIONS INC.

[2] ITRS, International Technology Roadmap for Semiconductors, http://www.itrs.net/, 2013.

[3] K. Cheemalapati, J. Keleher, Y. Li, Key chemical components in metal CMP slurries, Microelectronic Applications of Chemical Mechanical Planarization, Wiley Interscience, 2007, pp. 201-248.

[4] B. Vasilev, S. Bott, R. Rzehak, J.W. Bartha, Pad roughness evolution during break-in and its abrasion due to the pad-wafer contact in oxide CMP, Microelectronic Eng. 111 (2013) 21-28.

[5] P. Zantye, A. Kumar, A.K. Sikder, Chemical mechanical planarization for microelectronics applications, Materials Science and Engineering R: Reprots. 45(3) (2004) 89–220.

[6] J. Regh, G. Silvey, Method for Polishing a Silicon Surface, U.S. Patent 3,615,955, (1971), issued Oct. 26, 1971.

[7] T. Bibby, K. Holland, Equipment in Semiconductors and Semimetals, Volume 63, 1999, pp. 5-45.

[8] N. Shendon, Chemical Mechanical Polishing Apparatus with orbital Polishing, U.S. Patent 5,899,800, (1999), issued May 4, 1999.

[9] J. Adams, E. Smith, S. Schultz, Oscillating Orbital Polisher and Method, U.S. Patent 6,500,055, (2002), issued Dec. 31, 2002.

[10] K. Lee, Y. Lee, S. Kang, Method and Apparatus for Chemical mechanical Polishing, U.S. Patent 6,315,641, (2001), issued Nov. 13, 2001.

[11] M.R. Oliver, Chemical-mechanical planarization of semiconductor materials, Springer-Verlag, Berlin, 2004.

[12] R. DeJule, Contributing Editor, Semiconductor International, 10. http://www.semiconductor.net/article/CA6589952.html, 2008.

[13] D. T Asplund, Chemical Mechanical Paired Grinding, (2011).

[14] K.L. Johnson, Contact mechanics. Cambridge University Press, 1987.

[15] J.A. Greenwood, J.B.P.Williamson, Contact of Nominally Flat Surfaces, Proceedings of the Royal Society of London A, 295 (1966) 300- 319.

[16] C. Wang, P. Sherman, A. Chandra, A stochastic model for the effects of pad surface topography evolution on material removal rate decay in chemical-mechanical planarization, Semiconductor Manufacturing, IEEE Transactions, 18(4) (2005) 695-708.

[17] W. Che, Y. Guo, A. Chandra, A.F. Bastawros, A scratch intersection model of material removal during chemical mechanical planarization (CMP), Journal of manufacturing science and engineering, 127(3) (2005) 545-554.

[18] K.V. Shooter, D. Tabor, The frictional properties of plastics, Proceedings of the Physical Society, B, 65(9) (1952) 661.

[19] A. Bastawros, W. Che, A. Chandra, Measurement of Ultrathin Film Mechanical Properties by Integrated Nano-scratch/indentation Approach, Fundamentals of Nanoindentation and Nanotribology IV Book Series: Mat. Res. Soc. Symp. Proc. 1049 (2008) 57-62.

[20] J. Luo, D. Dornfeld, Material removal mechanism in chemical mechanical polishing: theory and modeling, Semiconductor Manufacturing, IEEE Transactions, 14(2) (2001) 112-133.

[21] F.W. Preston, The theory and design of plate glass polishing machines, J. Soc. Glass Technol. 11 (1927) 214-256.

[22] R.D. Mindlin, H. Deresiewicz, Timoshenko's shear coefficient for flexural vibrations of beams, No. TR-10, COLUMBIA UNIV NEW YORK, 1953.

[23] X. Sun, Z.J. Pei, X.J. Xin, M. Fouts, Waviness removal in grinding of wire-sawn silicon wafers: 3D finite element analysis with designed experiments, International Journal of Machine Tools and Manufacture, 44(1) (2004) 11-19.

[24] A.F. Bastawros, A. Chandra, Y. Guo, B. Yan, Pad effects on material removal rate in chemical-mechanical planarization, Journal of electronic materials, 31(10) (2002) 1022-1031.

[25] A.F. Bastawros, A. Chandra, S.D. Gouda, A Quantitative Analysis of Multi-scale Response of CMP Pad, Submitted ECS Journal of Solid State Science and Technology, (2016).

[26] A. Chandra, A.F. Bastawros, X. Wang, P. Karra, M. Haugen, An integrated wafer surface evolution model for chemical mechanical planarization (CMP), Micromanufacturing Processes, (2012) 373.

[27] W. Che, A. Bastawros, A. Chandra, P.M. Lonardo, Surface evolution during the chemical mechanical planarization of copper, CIRP Annals-Manufacturing Technology, 55(1) (2006) 605-608.

[28] W. Che, Y. Guo, A. Chandra, A.F. Bastawros, Mechanistic understanding of material detachment during micro-scale polishing, Journal of manufacturing science and engineering, 125(4) (2003) 731-5.

[29] A.Chandra,A.F.Bastawros,T.Yu,D.Asplund,Chemicalmechanicalpaired grinding: atoolformulti-wavelengthplanarization,TheInternationalJournal of AdvancedManufacturingTechnology(2016)1–7.

Table 1

Experimental Conditions for the PPP Parametric study.

	Contact Load F (N)	Transverse Feed Rate V_f (mm/s)	Wheel Speed V_s (rpm)	Slurry (μm)	Disc Material
F curve	4	0.21	500	1 alumina	Al
	8	0.21	500	1 alumina	Al
	14	0.21	500	1 alumina	Al
	18	0.21	500	1 alumina	Al
	16	0.21	500	0.05 silica	Al
	20	0.21	500	0.05 silica	Al
V_f curve	18	0.1	500	1 alumina	Al
	18	0.3	500	1 alumina	Al
	18	0.6	500	1 alumina	Al
	18	0.9	500	1 alumina	Al
V_s curve	20	0.21	200	1 alumina	Al
	20	0.21	300	1 alumina	Al
	20	0.21	500	1 alumina	Al
	20	0.21	600	1 alumina	Al
	20	0.21	500	1 alumina	Cu
	20	0.21	750	1 alumina	Cu
	20	0.21	1000	1 alumina	Cu
	20	0.21	1500	1 alumina	Cu
	20	0.21	2000	1 alumina	Cu